Report MDC Q0782

ADVANCED METHODS FOR PREPARATION AND CHARACTERIZATION OF INFRARED DETECTOR MATERIALS

S. L. Lehoczky

F. R. Szofran

McDonnell Douglas Research Laboratories
St. Louis, Missouri 63166

30 September 1981

Interim Report for the period 5 July 1980 – 30 September 1981
Contract NAS8-33107

Prepared for
George C. Marshall Space Flight Center
Marshall Space Flight Center, Alabama 35812

MCDONNELL DOUGLAS RESEARCH LABORATORIES

MCDONNELL DOUGLAS

CORPORATION

PREFACE

This report presents the results of research performed from 5 July 1980 through 30 September 1981 by the McDonnell Douglas Research Laboratories (MDRL) under the National Aeronautics and Space Administration Contract NAS8-33107 entitled "Advanced Methods for the Preparation and Characterization of Infrared Detector Materials." The ultimate objectives of the study are to quantitatively establish the characteristics of $Hg_{1-x}Cd_xTe$ as grown on Earth as a basis for subsequent evaluation of the material processed in space and to develop the experimental and theoretical analytical methods required for such evaluation.

The work was performed in the Solid State Sciences Department, managed by Dr. C. R. Whitsett. The principal investigator was Dr. S. L. Lehoczky; the co-investigator was Dr. F. R. Szofran. The technical manager was Mr. F. A. Reeves, Jr., NASA George C. Marshall Space Flight Center.

This report has been reviewed and is approved.

C. R. Whitsett
Chief Scientist-Solid State Sciences
McDonnell Douglas Research Laboratories

D. P. Ames
Staff Vice President
McDonnell Douglas Research Laboratories

For Val Fogle

F. A. Reeves, Jr.
Technical Manager
NASA George C. Marshall
Space Flight Center

CONTENTS

LIST OF ILLUSTRATIONS

LIST OF TABLES

1. INTRODUCTION

1.1 Scope of Study

The overall study includes the entire range, $0 < x < 1$, of $Hg_{1-x}Cd_xTe$ alloy compositions. Crystals will be prepared by the Bridgman-Stockbarger method with a wide range of crystal growth rates and temperature gradients adequate to prevent constitutional supercooling under diffusion-limited, steady-state, growth conditions. The longitudinal compositional gradients for different growth conditions and alloy compositions will be calculated and compared with experimental data to develop a quantitative model of solute redistribution during the crystal growth of the alloys. Measurements will be performed to ascertain the effect of growth conditions on radial compositional gradients. The pseudobinary HgTe-CdTe constitutional phase diagram was determined by precision differential-thermal-analysis measurements and used to calculate the segregation coefficient of Cd as a function of x and interface temperature. Experiments are being conducted and a theoretical analysis will be performed to determine the ternary phase equilibria in selected regions of the Hg-Cd-Te constitutional phase diagram. Electron and hole mobilities as functions of temperature are being analyzed to establish charge-carrier scattering probabilities. Computer algorithms specific to $Hg_{1-x}Cd_xTe$ are being developed for calculations of the charge-carrier concentrations, charge-carrier mobilities, Hall coefficient, and Fermi energy as functions of x, temperature, ionized donor and acceptor concentrations, and neutral defect concentrations.

1.2 Summary of Progress

1.2.1 Previously Reported Progress for the Period 5 December 1978 – 5 July 1980 (Reference 1)

A series of differential-thermal-analysis (DTA) measurements was performed for $Hg_{1-x}Cd_xTe$ alloy compositions with x = 0, 0.1, 0.2, 0.3, 0.4, 0.6, 0.7, 0.8, 0.9, and 1.0. The liquidus and solidus temperatures deduced from the DTA data were used to establish the pseudobinary HgTe-CdTe constitutional phase diagram.[1-3] The segregation coefficient of Cd was determined as a function of x and interface temperature.

Iterative phase-equilibrium calculations based on the regular associated solution (RAS) theory[4-5] were performed, and a set of RAS parameters was obtained by simultaneously least-squares-fitting the binary Hg-Te[6] and Cd-Te[7-9] and pseudobinary HgTe-CdTe phase diagrams. The RAS parameters were used to calculate the activities of Hg, Cd, and Te_2 and their partial pressures over pseudobinary melts.

$Hg_{1-x}Cd_xTe$ alloy crystals were grown by the Bridgman-Stockbarger method with constant furnace-translation rates of 0.0685 to 5.62 µm/s. For three $Hg_{0.8}Cd_{0.2}Te$ ingots, the longitudinal compositional profiles were determined by precision density measurements and were compared with calculated profiles[11] for various assumed values of D, the liquid HgTe-CdTe interdiffusion coefficient. The best fits to the data for the alloys with x = 0.2 yielded 5.5 x 10^{-5} cm^2/s for D and 1.5 x 10^6 K·s/cm^2 for G/R, the interface-temperature-gradient to growth-rate ratio required to prevent constitutional supercooling in the melt during crystal growth of $Hg_{0.8}Cd_{0.2}Te$ alloys.[1,3,12] Radial compositional variations were measured on thin slices from a series of ingots by infrared (IR) transmission-edge mapping. The radial compositional profiles deduced from the cut-on wavelengths implied concave solid/liquid interfaces for the entire lengths of the crystals.

Theoretical models and computer programs specific to $Hg_{1-x}Cd_xTe$ were developed for calculations of charge-carrier concentrations, Hall coefficient, Fermi energy, and conduction-electron mobility as functions of x, temperature, and ionized-defect and neutral-defect concentrations. As in previous work on the HgCdSe alloy system,[13,14] the Kane three-band model[15] was used to describe the band structure of the HgCdTe alloys, and the best available band parameters were compiled from the literature. The temperature dependence of the electron concentration was calculated for various net donor concentrations from 4.2 to 300 K, and the calculated results agree well with available experimental data.[1]

The mobility calculations included the following instrinsic scattering mechanisms: longitudinal-optical phonon, longitudinal- and transverse-acoustical phonon, heavy-hole, and alloy disorder potential. The extrinsic scattering mechanisms included charge and neutral point-defects. A comparison of calculated results with available experimental data indicate that longitudinal-optical phonon, and charged and neutral defect scattering are the dominant mobility-limiting mechanisms.

2

1.2.2 Progress for the Current Period: 5 July 1980 - 30 September 1981

A series of differential-thermal-analysis measurements was performed for $(Hg_{1-x}Cd_x)_yTe_{1-y}$ alloy compositions with $x = 0.091$ and $y = 0.648$; $x = 0.100$ and $y = 0.550$ and 0.591; $x = 0.200$ and $y = 0.544, 0.554, 0.60$, and 0.952; $x = 0.299$ and $y = 0.544$ and 0.589; and $x = 0.401$ and $y = 0.545$. The DTA data were used to establish the liquidus temperatures for the alloy compositions.

The pseudobinary data obtained during the previous funding period were re-fitted to a set of empirical equations to obtain more accurate expressions for the segregation coefficient of Cd as a function of x and interface temperature than was given in Reference 1. Preliminary theoretical analysis was performed to establish the ternary phase equilibrium parameters for the metal-rich region of the phase diagram. Pseudobinary HgTe-CdTe phase equilibrium calculations were performed to determine the sensitivity of the thermodynamic fitting parameters to various assumptions used in the calculational models.[1,4,5]

$Hg_{0.8}Cd_{0.2}Te$ alloy crystals were grown by a Bridgman-Stockbarger method at constant furnace-translation rates of 0.241, 0.245, and 0.247 μm/s, and a $Hg_{0.7}Cd_{0.3}Te$ alloy crystal was grown at a furnace translation rate of 0.231 μm/s. The lower-zone temperatures ranged from 175 to 600°C, and the upper-zone temperatures ranged from 810 to 920°C. Radial compositional variations were measured on thin slices from the ingots by infrared transmission mapping. Similar measurements were performed for an ingot grown during the previous contractual period. The radial alloy homogeneities of the ingots showed a strong correlation to the growth parameters employed. The variation of the radial compositional distributions with changes in the upper- and lower-zone temperatures suggests significantly higher thermal conductivities in the melt than in the solidified alloys.

Galvanomagnetic measurements were performed to expand the data base for well-characterized, homogeneous HgCdTe crystals. Using the van der Pauw technique, Hall coefficient and resistivity measurements from 10 to 300 K were performed on slices, taken from a 1C-mm and a 5-mm diameter ingot. For a number of slices the measurements were repeated following annealing in a mercury atmosphere at several temperatures. Theoretical analyses were performed to estimate point-defect concentrations in n-type samples.

1.3 Formal Reports, Publications, and Presentations:

1.3.1 Research Funded Under Contract NAS9-33107:

- F. R. Szofran and S. L. Lehoczky, "The HgTe-CdTe Pseudobinary Phase Diagram", 22nd Annual Electronic Materials Conference, Ithaca, New York, 24-27 June 1980.

- S. L. Lehoczky, F. R. Szofran, and B. G. Martin, "Advanced Methods for Preparation and Characterization of Infrared Detector Materials", McDonnell Douglas Corporation Report MDC Q0717 (5 July 1980), Final Report for the period 5 December 1978 - 5 July 1980 for the George C. Marshall Space Flight Center Contract No. NAS8-33107.

- S. L. Lehoczky and F. R. Szofran, "Directional Solidification and Characterization of $Hg_{1-x}Cd_xTe$ Alloys", Materials Research Society Symposium - Materials Processing Research in the Reduced Gravity Environment of Space, Boston, Massachusetts, 16-18 November 1981 (accepted).

- S. L. Lehoczky and F. R. Szofran, "Diffusion-Limited Directional Solidification of $Hg_{0.8}Cd_{0.2}Te$", Fifth International Conference on Vapor Growth and Epitaxy and Fifth American Conference on Crystal Growth, Coronado, California, 19-24 July 1981.

1.3.2 Research Funded in Part Under Contract NAS8-33107

- F. R. Szofran and S. L. Lehoczky, "The Pseudobinary HgTe-CdTe Phase Diagram", J. Electron. Matl. (in press).

- S. L. Lehoczky, C. J. Summers, and F. R. Szofran, "Directional Solidification and Characterization of $Hg_{1-x}Cd_xTe$ (x < 0.25)," NATO Cadmium Mercury Telluride (CMT) Workshop, Grenoble, France, 23-24 April 1981.

- S. L. Lehoczky, F. R. Szofran, C. J. Summers, and B. G. Martin, "Electrical Characterization of $Hg_{1-x}Cd_xTe$ Alloys", Materials Research Society Symposium – Materials Processing Research in the Reduced Gravity Environment of Space, Boston, Massachusetts, 16-18 November 1981 (accepted).

2. TERNARY Hg-Cd-Te PHASE DIAGRAM

Differential-thermal-analysis (DTA) measurements were performed for a series of $(Hg_{1-x}Cd_x)_yTe_{1-y}$ ternary alloy compositions. The DTA data were used to establish the liquidus temperatures for selected regions of the Hg-rich segment of the constitutional phase diagram.

2.1 Alloy Preparation

With the exception of Te preparation, the procedure for the preparation of the constituent elements and the casting of the alloys was the same as described in Reference 1. For the present study, in contrast to the previous procedure, the Te charge was prepared by crushing large Te ingots in an agate mortar in a dry nitrogen atmosphere. No further material processing was performed.

The alloy compositions that were prepared and the alloy compositions for which satisfactory liquidus data were obtained are summarized in Figure 1.

Figure 1. $(Hg_{1-x}Cd_x)_yTe_{1-y}$ samples prepared.

6

2.2 Experimental Method for Differential Thermal Analysis

Except for data acquisition and recording, the experimental arrangement and procedure were similar to those described in Reference 1. A block diagram of the present data acquisition and recording system is shown in Figure 2. The type-K chromel-alumel thermocouples used previously[1] were replaced by more-stable type-S (Pt/Pt-10Rh) thermocouples. The triple-point-of-water cell and x-y recorder of the previous experimental arrangement were replaced by a data logger (Fluke 2240B) with isothermal, thermally-compensated junctions and a microcomputer (Digital Equipment Corp. MINC-1) The melting point of antimony (Sb) was used as the temperature calibration point during each experimental run. A typical DTA curve obtained by using the new data acquisition arrangement is shown in Figure 3.

2.3 Differential Thermal Analysis Results for the Hg-Rich Region of the Ternary System

Successful DTA measurements were performed for the $Hg_{0.495}Cd_{0.055}Te_{0.450}$, $Hg_{0.435}Cd_{0.109}Te_{0.456}$, $Hg_{0.443}Cd_{0.111}Te_{0.446}$, $Hg_{0.381}Cd_{0.163}Te_{0.456}$, $Hg_{0.326}Cd_{0.219}Te_{0.455}$, $Hg_{0.532}Cd_{0.059}Te_{0.409}$, $Hg_{0.481}Cd_{0.120}Te_{0.399}$, $Hg_{0.413}Cd_{0.176}Te_{0.411}$, $Hg_{0.589}Cd_{0.059}Te_{0.352}$, and $Hg_{0.762}Cd_{0.190}Te_{0.048}$ alloy compositions. As implied by Figure 1, a substantial number of prepared ampules were discarded for various reasons. The measured liquidus temperatures, elemental masses, and free volumes inside the ampules are summarized in Table 1.
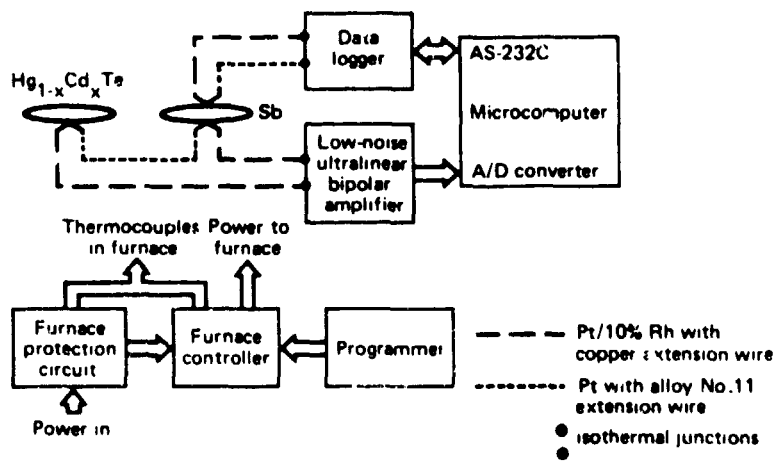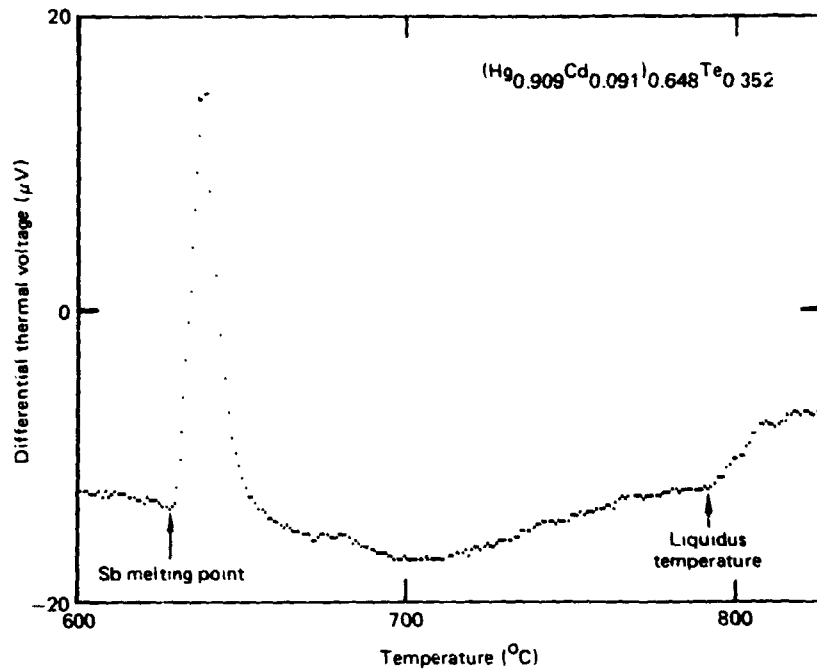

Figure 2. Electronic instrumentation for differential thermal analysis.

$(Hg_{0.909}Cd_{0.091})_{0.648}Te_{0.352}$

Sb melting point

Liquidus temperature

GP11-0818-9

Figure 3. Typical differential-thermal-analysis record.

TABLE 1. LIQUIDUS TEMPERATURES FOR Hg-RICH
$(Hg_{1-x}Cd_x)_yTe_{1-y}$ ALLOYS.

Overall x	Overall y	Observed liquidus ($^\circ C$)	Free volume inside ampule (%)	Mass of Hg (g)	Mass of Cd (g)	Mass of Te (g)
0.100	0.550	751 ± 3	20	10.344	0.644	5.986
0.100	0.591	773 ± 4	19	10.206	0.636	5.000
0.091	0.648	788 ± 4	22	11.532	0.649	4.380
0.200	0.544	823 ± 3	23	8.809	1.233	5.862
0.200	0.554	819 ± 3	33	8.724	1.222	5.580
0.200	0.601	849 ± 4	17	9.384	1.311	4.943
0.200	0.952	806 ± 5	32	14.394	2.018	0.581
0.299	0.544	868 ± 4	19	7.701	1.836	5.847
0.299	0.589	895 ± 4	17	8.094	1.938	5.120
0.401	0.545	907 ± 4	30	6.465	2.423	5.727

GP11-0818-1

Because the partial vapor pressures of Hg over the alloy melts are ex-
pected to be much larger than the partial pressures of Cd and Te,[1] the prefer-
ential evaporation of mercury into the ampule free volume alters both the
Te/metal and Cd/Hg fractions. Hence, the actual melt compositions at the
liquidus are somewhat higher in x and somewhat lower in y than the values

8

listed in Table 1. The precise melt compositions cannot be calculated from the masses of the elements and the free volume in an ampule because of the lack of vapor pressure data for metal-rich melts and a realistic thermodynamic model for the ternary system (see Section 3).

The major recognized sources of error in the liquidus temperature data are the uncertainty in the temperature measurements and the subjectivity in selecting the proper liquidus points from the DTA curves. Estimates of the uncertainties associated with the temperature measurements were obtained from calibration runs using an ampule containing silver as a DTA sample. The calibration runs indicated a maximum discrepancy of $1.5^{\circ}C$ between the actual melting temperature of silver ($961.93^{\circ}C$) and the value measured relative to the melting temperature of Sb in the DTA apparatus. The DTA signals were recorded at $1^{\circ}C$ intervals, which implied an additional inherent uncertainty of $\pm 0.5^{\circ}C$. Thus, the uncertainties arising from temperature measurements ranged from about $\pm 0.5^{\circ}C$ at the melting point of Sb ($630.74^{\circ}C$) to about $\pm 2^{\circ}C$ at the melting point of Ag.

2.4 Liquid-Solid Equilibrium Parameters for the Pseudobinary Alloy System

The pseudobinary data obtained during the previous funding period[1,2] were reanalyzed to obtain more exact expressions for the compositional and temperature dependences of the Cd segregation coefficient than were given in Reference 1. The new empirical expressions for the solidus curve of the phase diagram are

$$x^S(T) = C_1 \sin \left(\frac{\pi}{2} T^*\right) + C_2 \sin \left(\frac{\pi}{2} T^{*1/2}\right) + C_3 \log_{10} (9T^* + 1)$$

$$+ C_4 T^{*1/2} \qquad (T > 690^{\circ}C) \qquad (1a)$$

and

$$x^S(T) = x^S (690^{\circ}C) (T - 670^{\circ}C)/20^{\circ}C \qquad (670^{\circ}C < T < 690^{\circ}C). \qquad (1b)$$

9

The functional form for the liquidus curve remains

$$x^L(T) = D_1 T^* + D_2 T^{*2} + D_3 T^{*3} + D_4 T^{*4}, \tag{2}$$

where $T^* = (T - 670^{\circ}C)/412^{\circ}C$ and the least-squares fit values for the C_i and D_i are given in Table 2. Figures 4-7 are revisions based upon Equations (1) and (2) of Figures 8, 10, 11, and 13, respectively in Reference 1.

TABLE 2. VALUES FOR THE CONSTANTS C_i AND D_i IN EQUATIONS 1 AND 2.

i	C_i	D_i
1	0.502804	0.607640
2	0.165390	0.077209
3	0.746318	0.696167
4	−0.413546	−0.381683

GP11-0818-2
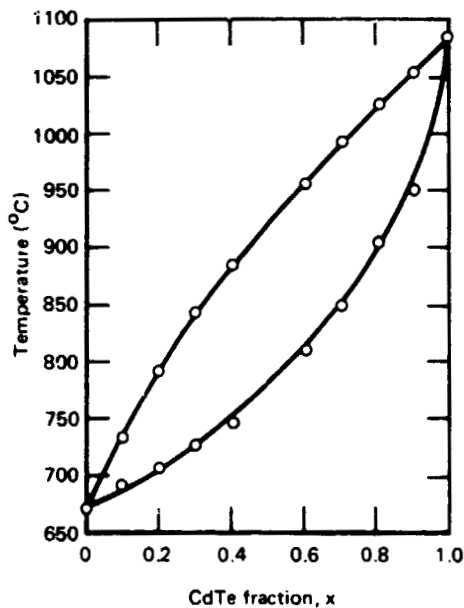
Figure 4. $Hg_{1-x}Cd_x Te$ phase diagram.
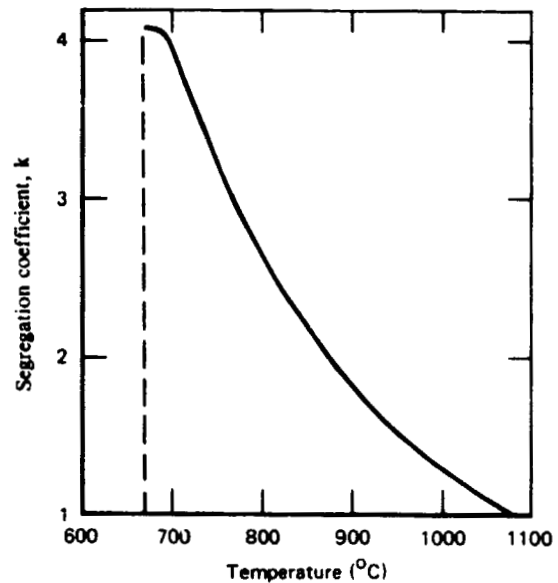
GP11-0818-10

Figure 5. Temperature dependence of the CdTe segregation coefficient.

GP11-0818-11

10

Figure 6. Composition dependence of the CdTe segregation coefficient.

Figure 7. The temperature dependence of the rate of change with respect to temperature of the alloy liquid fraction for various alloy compositions.

11

3. PHASE EQUILIBRIUM CALCULATIONS

Preliminary calculations were performed to establish correlations between the measured ternary liquidus data and the regular-associated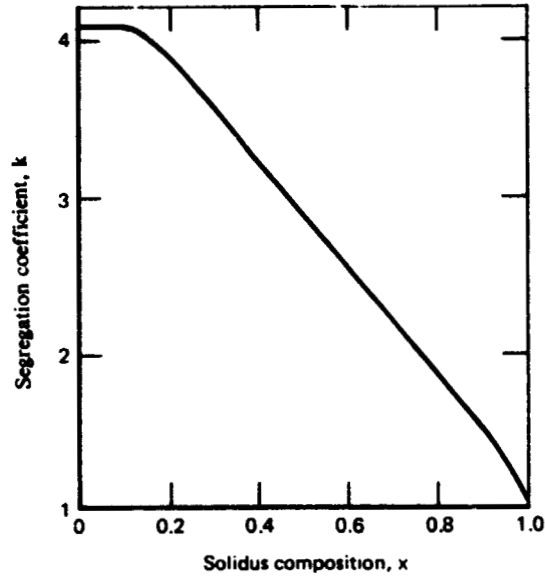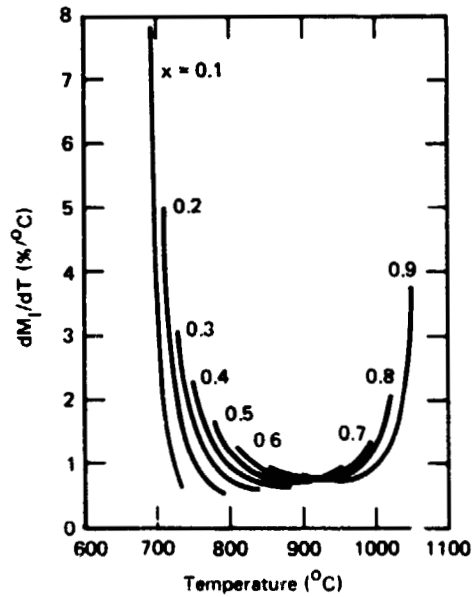-solution (RAS) thermodynamic parameters established previously. The comparisons between the measured and calculated results suggested significantly larger values for both w (the interaction parameter between Hg and Cd in the melt) and W (the interaction parameter between HgTe and CdTe in the solid phase) than were obtained by least-squares-fitting the HgTe-CdTe pseudobinary phase diagram data.[1] Consequently, additional pseudobinary phase-equilibrium calculations were performed to determine the sensitivity of the thermodynamic fitting parameters to assumptions about the structure in the HgTe-CdTe melts and evaluate the validity of some of the approximations of the RAS theory when applied to the thermodynamic modeling of the Hg-Cd-Te alloy system.

Calculations were performed for two sets of assumptions: (1) HgTe is a completely dissociated regular solution and CdTe is a regular associated solution, and (2) HgTe is a completely dissociated regular solution and CdTe is a completely associated regular associated solution. A review of the results of these calculations and of the mathematical approaches used in the development of the RAS formalisms[4,5,16] suggests that because of the approximations used, the RAS models used previously are inadequate, without major revisions, to correctly describe the thermodynamic behavior of the complete ternary alloy system.
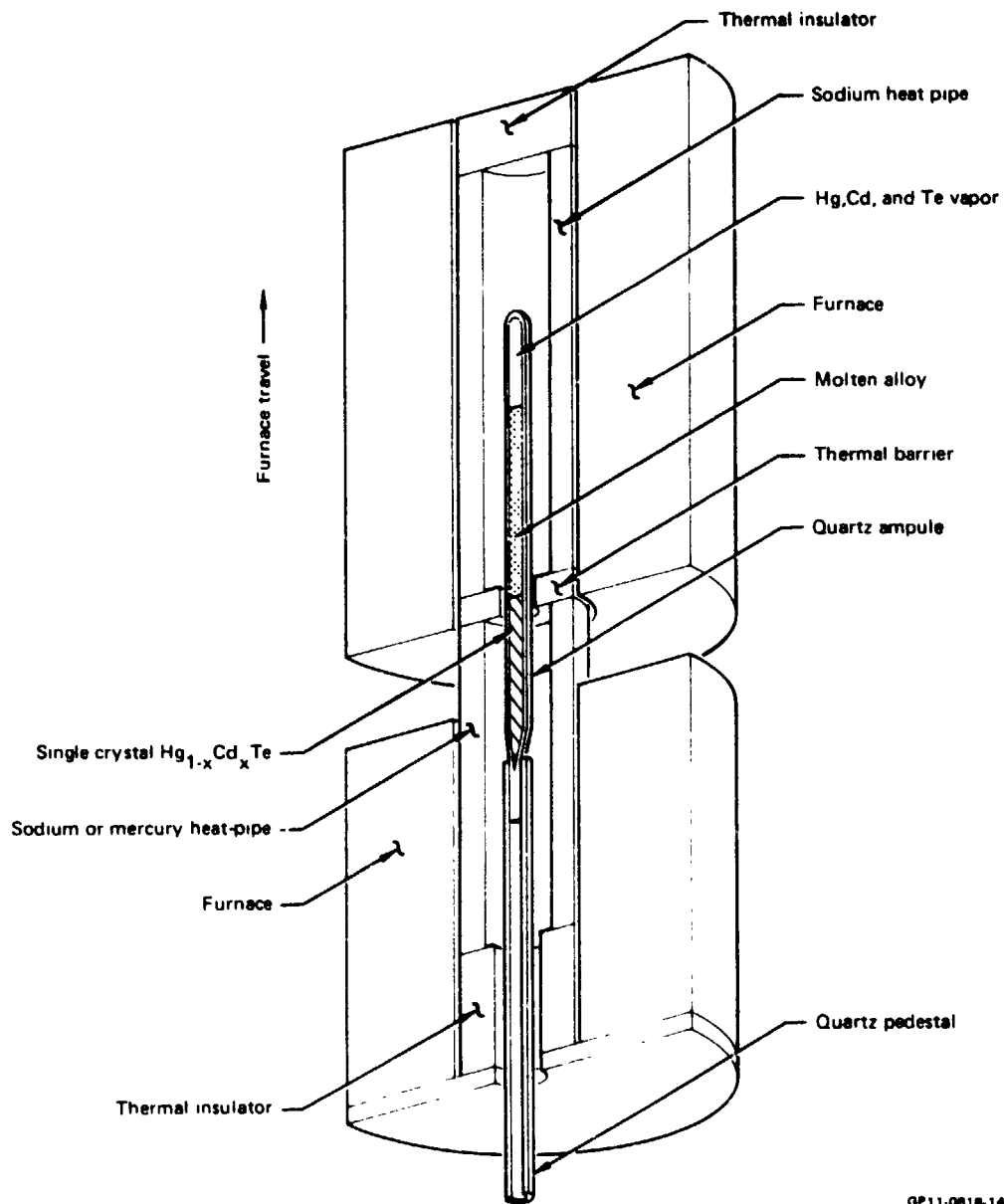
4. DIRECTIONAL SOLIDIFICATION OF $Hg_{1-x}Cd_xTe$
ALLOYS FROM PSEUDOBINARY MELTS

4.1 Alloy Preparation and Crystal Growth Runs

Three $Hg_{0.8}Cd_{0.2}Te$ and one $Hg_{0.7}Cd_{0.3}Te$ alloy ingots were prepared by reacting 99.9999% pure elemental constituents in sealed, evacuated, fused-quartz tubing. The tubing dimensions were 5-mm i.d. x 10-mm o.d. The ampules were prepared and loaded, and the alloys were reacted as described in Reference 1 and Section 2.1.

The precast alloys were regrown by unidirectional solidification in the growth apparatus illustrated in Figure 8. The details of the experimental arrangement and procedures are described in Reference 1.

Crystal growth runs were completed for ampules L13, L14, L15, and L16 at furnace translation rates of 0.241, 0.231, 0.245, and 0.247 $\mu m/s$, respectively. For ingot L16, the growth was stopped and the melt was quenched when about half of the alloy was crystallized to demarcate the shape of the growth interface. The longitudinal temperature profiles in the furnace prior to growth initiation are shown in Figures 9-12. The pertinent growth parameters are summarized in Table 3. Ingots L6 and L7 were grown during the previous contracting period and are repeated here for the purposes of later discussions. The longitudinal temperature profile in the furnace prior to the growth of ingots L6 and L7 is shown in Figure 13.

Thermal insulator

Sodium heat pipe

Hg,Cd, and Te vapor

Furnace

Molten alloy

Thermal barrier

Quartz ampule

Quartz pedestal

Single crystal $Hg_{1-x}Cd_xTe$

Sodium or mercury heat-pipe

Furnace

Thermal insulator

Furnace travel

GP11-0618-14

Figure 8. Bridgman-Stockbarger crystal-growth furnace assembly.

14

Figure 9 Temperature profile of crystal-growth furnace during growth of ingot L13.

Figure 10. Temperature profile of crystal-growth furnace during growth of ingot L14.

Figure 11. Temperature profile of crystal growth furnace during growth of ingot L15.
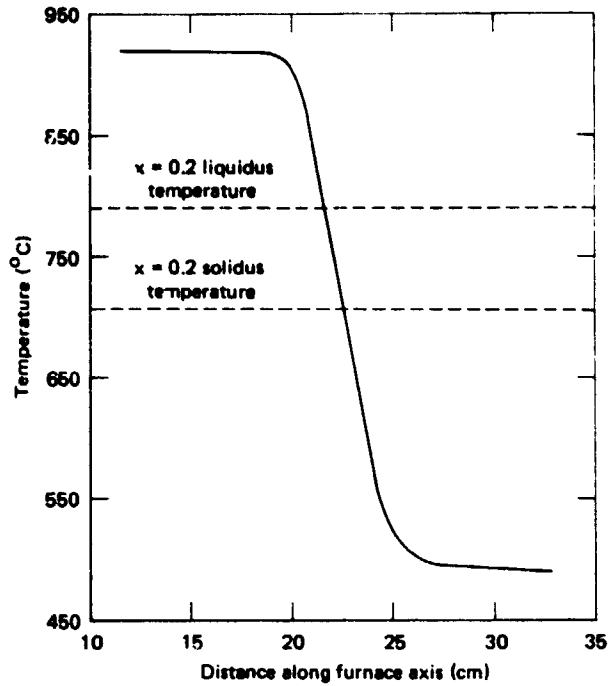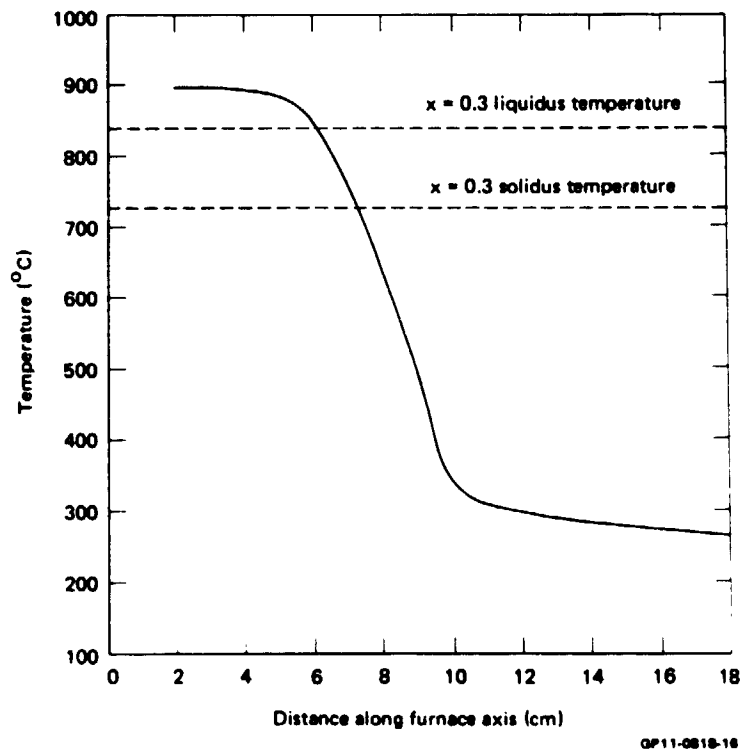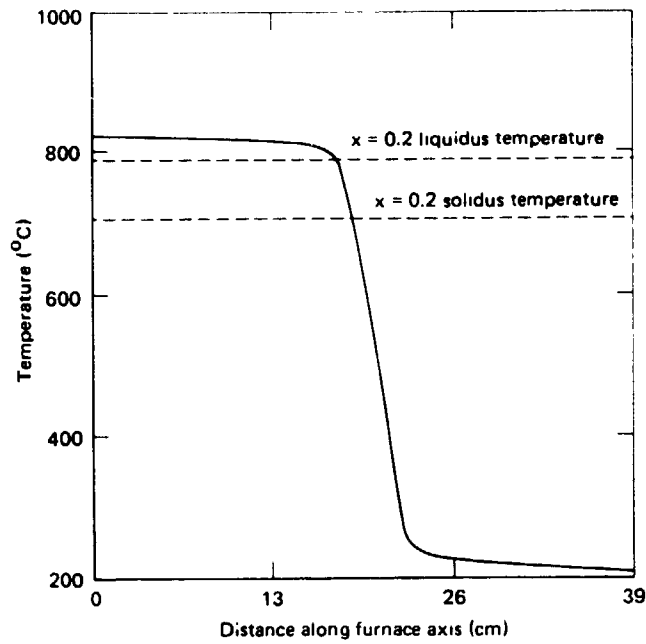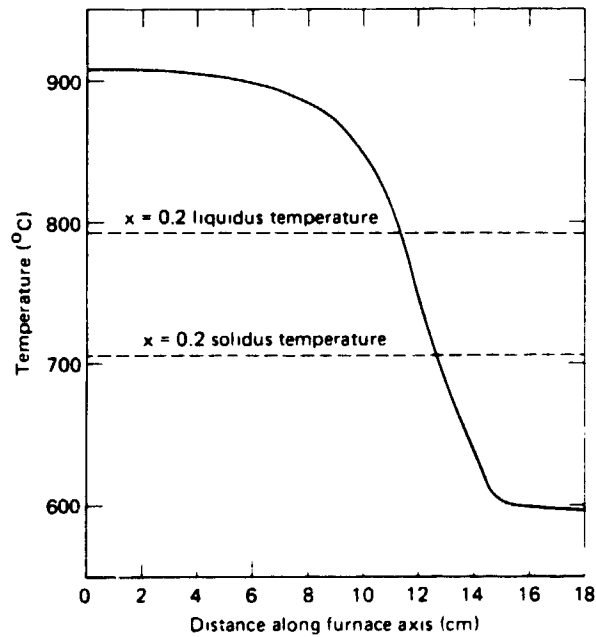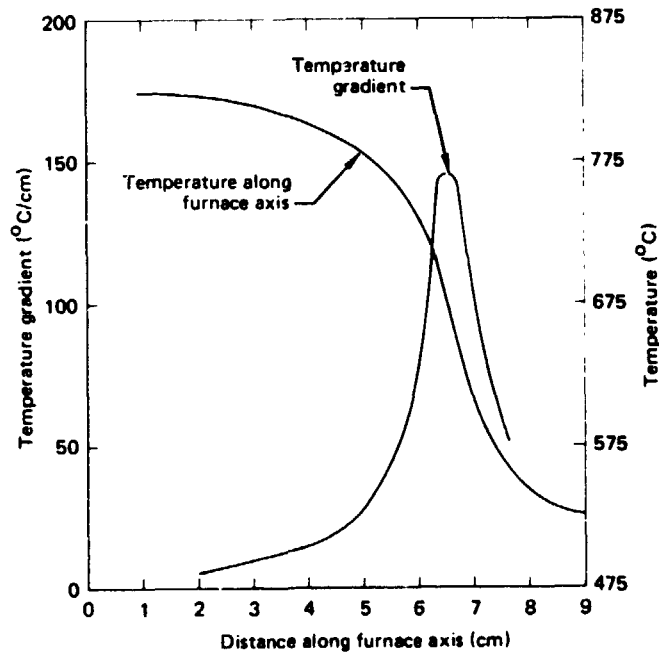

Figure 12. Temperature profile of crystal-growth furnace during growth of ingot L16.

TABLE 3. CRYSTAL-GROWTH SAMPLES AND GROWTH CONDITIONS.

Sample designation	Composition, x	Lower zone temperature (°C)	Upper zone temperature (°C)	Thermal barrier width (cm)	Growth rate (μm/s)
L6	0.202	520	820	0.4	0.310
L7	0.202	520	820	0.4	0.068
L13	0.200	493	919	3.8	0.241
L14	0.303	175	897	3.8	0.231
L15	0.202	200	810	3.8	0.245
L16[+]	0.198	600	910	3.8	0.247

[+]Growth stopped and melt quenched about halfway through growth

GP11-0818-3

Figure 13. Temperature profile of crystal-growth furnace during growth of ingots L6 and L7.

4.2 Infrared Transmission Measurements

Thin (≈ 200 - 300 μm) slices from ingots L7, L13, L14, L15, and L16 were prepared for evaluation of radial compositional variations by infrared transmission-edge mapping. The transmission measurements were made at room temperature through 1-mm diameter areas at regulary spaced locations on each slice.

17

Initially, slices from ingot L16 were essentially opaque to infrared radiation because of the highly p-type character of the slices. The slices were subsequently annealed in mercury vapor to reduce the hole carrier concentrations and thus to enhance infrared transmission.

The infrared cut-on wavelengths along the growth axis, the corresponding alloy compositions, and the radial variations of the alloy compositions are summarized for ingot L7 in Table 4. Typical results for the radial variation of the cut-on wavelengths and corresponding alloy compositions for slices cut from ingots L13, L14, and L16 are shown in Figures 14-16.

TABLE 4. COMPOSITIONAL VARIATIONS ALONG THE GROWTH
AXIS OF INGOT L7.

Slice designation	Distance from tip (cm)	Cut-on wavelength (μm)	Composition, x	Compositional variation across slice, Δx
L7-17	1.57	$2.75^{+0.05}_{-0.10}$	0.416	0.008
L7-30	3.16	4.10 ± 0.025	0.310	0.0012
L7-57	5.70	503 ± 0.025	0.270	0.0008
L7-97	9.54	7.65 ± 0.10	0.212	0.0014
L7-119	11.66	14.2	0.160	—
L7-141	14.17	No observable transmission through slice		
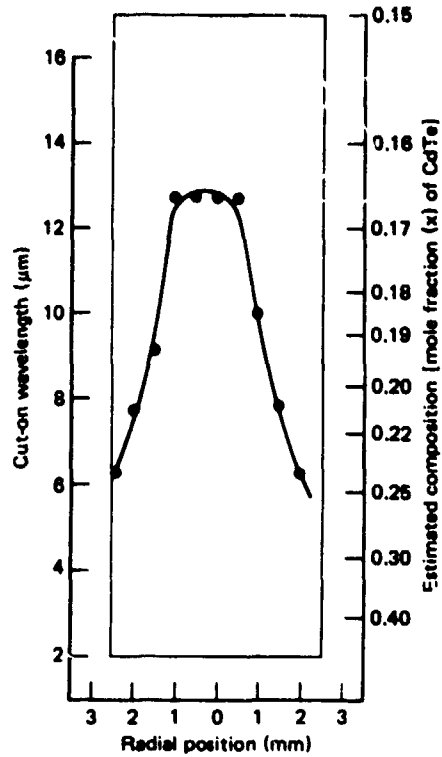
Figure 14. Typical radial variation of the cut-on wavelength and Cd
composition for a slice cut from ingot L13.
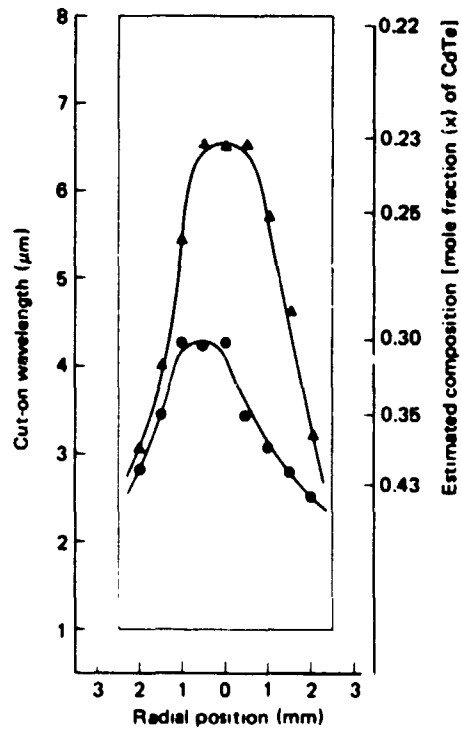
Figure 15. Typical radial variations of the cut-on wavelength and Cd
composition for slices cut from ingot L14.
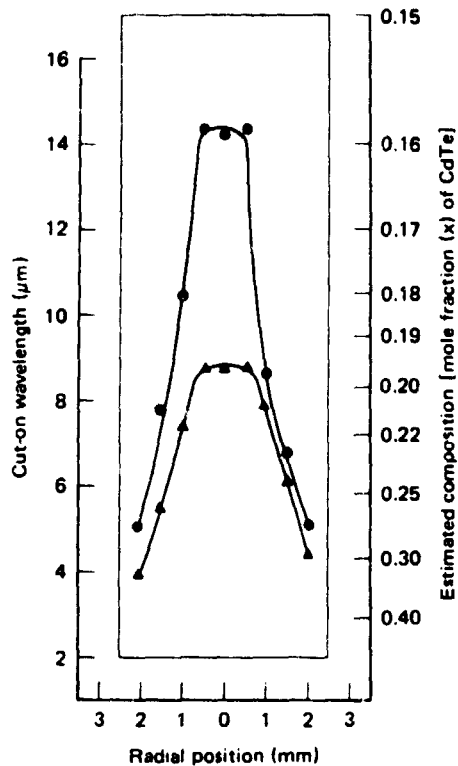
Figure 16. Typical radial variations of the cut-on wavelength and Cd composition for slices cut from ingot L16.

4.3 Discussion of Results

As indicated by the data in Table 4, the infrared measurements indicated a high degree of radial compositional uniformity for more than half of the 18-cm growth length of ingot L7. For about 9 cm of the ingot length, the radial variation in the CdTe mole fraction, x, was within ± 0.0015 over entire wafers. Ingot L7 was grown using a relatively slow growth rate (0.0685 μm/s) and a rather thin (0.4 cm) thermal barrier. For the preselected upper-zone temperature of 820°C, an appropriate value for the lower-zone temperature, T_L, was calculated from

$$T_U^4 - T_I^4 = T_I^4 - T_L^4 , \tag{3}$$

where T_I is the growth interface temperature for an alloy composition of x = 0.2 and T_U is the upper-zone temperature. Equation (3) represents the

20

condition for radiative heat balance at the middle of the thermal barrier for the case of equal values for the pertinent emissivities.

For comparison with the results for ingot L7, the radial compositional variations along the growth axis of ingot L6 are reproduced from Reference 1 in Figure 17. The growth parameters for ingot L6 were the same as for ingot L7 except for the growth rate of 0.31 μm/s, which was about four times larger than that for ingot L7. In contrast to ingot L7, ingot L6 showed significant radial compositional variations for the entire growth length. The observed radial compositional profiles for the ingot indicate a concave solid/liquid interface during the growth of ingot L6.

Apparently, the large differences in the radial compositional homogeneities of ingots L6 and L7 are related to the different growth rates involved. The characteristic diffusion length that governs the longitudinal solute (CdTe) redistribution in the melt during the growth of a crystal is inversely proportional to the growth (furnace translation) rate (see, for example, References 1 and 11). The magnitude of the longitudinal solute concentration
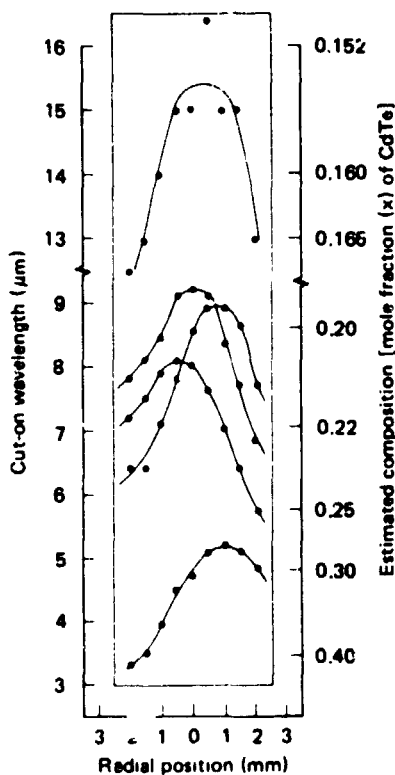
GP11-0818-23

Figure 17. Radial variations of the cut-on wavelength and Cd composition for ingot L6.

21

gradient is inversely proportional to the diffusion length and thus directly proportional to the growth rate. Consequently, the longitudinal compositional gradients in the melt just ahead of the interface during the growth of ingot L6 were substantially larger than those during the growth of ingot L7. The comparison of the compositional data for ingots L6 and L7 therefore suggests a strong correlation between radial compositional redistribution and the magnitude of the longitudinal alloy gradient in the melt ahead of the growth interface.

Because the HgTe-rich component rejected during the Bridgman-Stockbarger growth of the alloys is more dense than the original melt, the melt ahead of the growth interface should be gravitationally stable against convection if a flat growth interface is maintained during the growth process. However, because the liquidus and solidus boundaries of the $Hg_{1-x}Cd_xTe$ pseudobinary constitutional phase diagram are widely separated, the growth interface temperature undergoes large changes during the crystal growth,[1] thereby making a curved isotherm at the solidification temperature unavoidable at some point during the growth process. This curved isotherm can readily lead to a curved (concave or convex) solid-liquid interface, which need be neither an isotherm nor an isoconcentrate. Consider the case of a concave liquid interface. The rejected HgTe-rich liquid will tend to flow along the interface under the influence of gravity, resulting in a higher HgTe concentration at the center than at the edges of the interface. Because the alloy solidus temperature decreases with increased HgTe concentration, the interface temperature at the center will be decreased with respect to the edges, causing the interface to become more concave. Similar considerations apply to a convex liquid interface. Lateral diffusion tends to drive the interfacial melt compositions to some equilibrium condition. For a given interface radius of curvature, the condition for the onset of an interfacial fluid flow should be directly related to the initial longitudinal compositional gradient in the melt and hence to the growth rate. It is likely therefore that the large disimilarities in the radial alloy compositional distributions in ingots L6 and L7 are a direct consequence of differences in the gravity-induced interfacial fluid flows.

To ascertain the effects of variations in the thermal barrier width (see Figure 8) on radial alloy homogeneity, ingots L13, L14, L15, and L16 were grown using thermal barrier widths of 3.8 cm in contrast to the barrier widths

of 0.4 to 0.8 cm employed previously. Similarly to the case of ingot L6, the radial compositional profiles for each ingot indicate concave solid/liquid interfaces for the entire growth length and thus significant radial temperature gradients in the vicinity of the interface.

Approximate calculations were performed for the temperature distribution in the vicinity of the growth interface for various assumed values for the liquid and solid thermal conductivities. Although the validity of some of the approximations used is suspect, the qualitative dependence of the calculated radial temperature distribution on the upper- and lower-zone temperatures suggest that the thermal conductivity in the liquid just ahead of the growth interface is higher than in the resolidified alloys. This result contrasts with previous assumptions that the thermal conductivity of the solid is higher generally than that of the melt.[17]

Although ingot L7 showed a high degree of radial homogeneity, the ingot was polycrystalline. Similar results also have been seen for crystals grown at MDRL under the McDonnell Douglas Corporation Independent Research and Development (IRAD) program. Since grain selection is usually favored by convex interface shape,[16] the growth of high-quality $Hg_{1-x}Cd_xTe$ crystals by the Bridgman-Stockbarger method may require a curved growth interface, which is likely to be unstable against gravity-induced convective fluid flows.

5. ELECTRICAL CHARACTERIZATION

Galvanomagnetic measurements were performed to expand the data base for well-characterized, homogeneous HgCdTe cyrstals. Measurements were made on slices cut from ingot L7, described in tne previous section and on slices cut from a 10-mm diameter ingot (L0721-51) that was grown for the McDonnell Douglas Corporation IRAD program. Ingot L0721-51 was grown by the Bridgman-Stockbarger method and was radially homogeneous ($\Delta x < 0.005$) for a 70-mm length over which x increased monotonically from 0.27 to 0.32. For a number of slices, the measurements were repeated following annealing in a Hg atmosphere at several temperatures. Theoretical analyses were performed to estimate point defect concentrations in a typical sample from ingot L7.

5.1 Sample Preparation and Screening

The samples used for the measurements were sliced from the ingots with a wire saw using a slurry of 600-mesh SiC, water, and glycerin. The plane of each slice was perpendicular to the growth axis. To remove surface damage caused by slicing, the samples were etched in a Br_2-methanol solution.

The alloy compositional variations and the overall alloy composition for each sample were deduced from infrared transmission cut-on measurements as described in Section 4.2. Table 5 summarizes the compositional characteristics for samples for which data are reported.

TABLE 5. ALLOY COMPOSITIONS AND COMPOSITIONAL VARIATIONS OF SAMPLES USED FOR ELECTRICAL CHARACTERIZATIONS.

| Sample	Composition, x	Composition variation, Δx
L7-57	0 270	0.0008
L0721-51-49	0.326	0.005
L0721-51-82	0.284	0.0015
L0721-51-113	0.274	0.004

GP11 0818-5

5.2 Electrical Resistivity and Hall Coefficient Measurements

The electrical resistivity and Hall coefficient measurements were made by the method of van der Pauw.[8] Following attachment of the electrical leads with indium, the samples were fastened to the sample block of a closed-cycle helium refrigerator, which is an integral part of an MDRL-designed automated galvanomagnetic data acquisition system. A block diagram of the system is shown in Figure 18. The entire experiment, including temperature variations and magnetic field direction, is controlled by a microcomputer (Digital Equipment Corp. MINC-11).

The temperature dependence of the electron concentration for a sample from ingot L7 (L7-57) is shown in Figure 19. The sample was n-type and had a net donor concentration, N_D-N_A, of 5.9×10^{15} cm^{-3}. Ingots grown at high lower-zone temperatures ($\gtrsim 450^\circ$C) tend to be p-type. The lower-zone temperature during the growth of ingot L7 was about 520°C. However, following growth, the zone temperature was reset to 270°C, and the ingot was annealed at that temperature for about 340 h.

Following the initial measurements, sample L7-57 was annealed in mercury vapor, and measurement of the temperature dependence of the electrical proper-
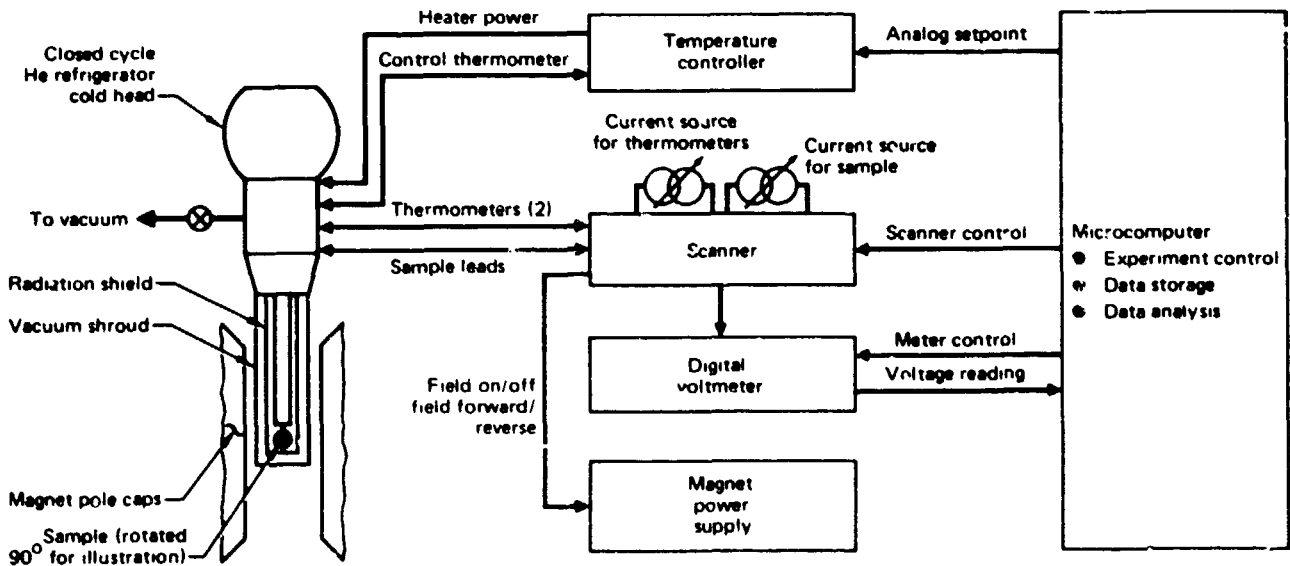
Figure 18. Block diagram of automated system for measurements of galvanomagnetic properties of semiconductors.
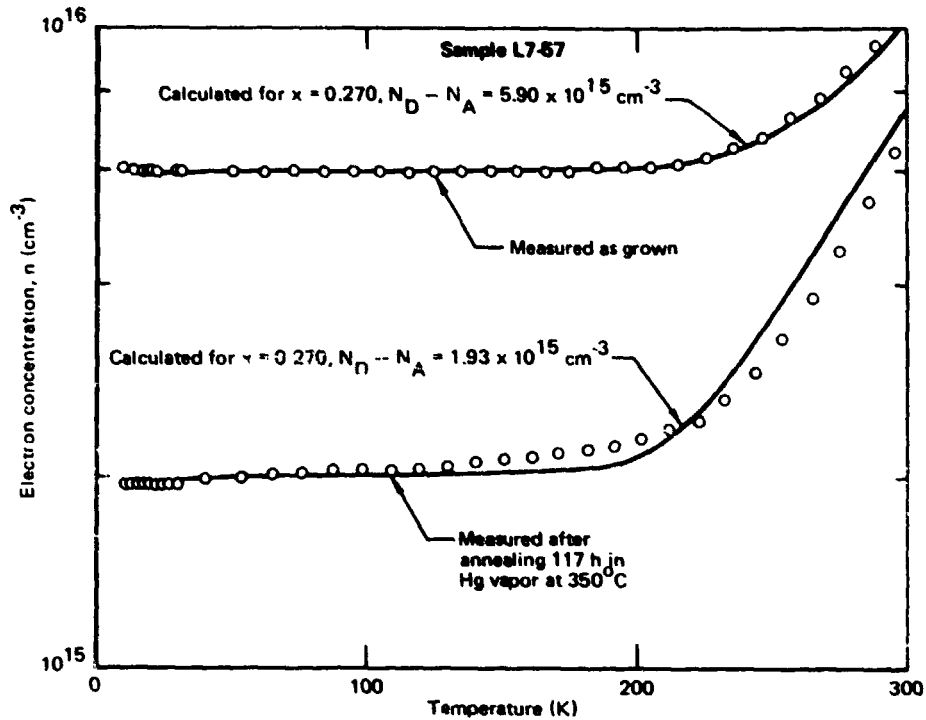
25

Figure 19. Electron concentration as a function of temperature for sample L7-57.

ties was repeated. The annealing conditions are given in Table 6. The temperature dependence of the carrier concentration in the sample following annealing is also shown in Figure 19.

The solid curves shown in Figure 19 were calculated using the theoretical model and band parameters described in Reference 1. The calculated results agree remarkably well with the experimental data, especially for the as-grown condition.

The measured and calculated[1] electron mobilities for the as-grown sample L7-57 are shown in Figure 20. The various curves illustrate the relative variations of the calculated mobilities with alloy-disorder energy and acceptor concentrations. The best fit to the temperature dependence of the mobility suggests an alloy-disorder energy of 3.5 - 4.5 eV, about a factor of two higher than the expected value[1] of ~ 2 eV. The best fit to the data for an alloy-disorder energy of 3 eV implies a donor concentration of 8.9×10^{15} cm^{-3} and an acceptor concentration of 3.0×10^{15} cm^{-3}.

26

**TABLE 6. Hg-VAPOR ANNEALING CONDITIONS FOR SAMPLES
USED FOR ELECTRICAL CHARACTERIZATIONS**

| Annealing run	Annealing time (h)	Annealing temperature (°C)	Ingot slices			
			L7-57	L0721-51-49	L0721-51-82	L0721-51-118
A1	385	323	–	X	–	X
A2	117	350	X	X	–	X
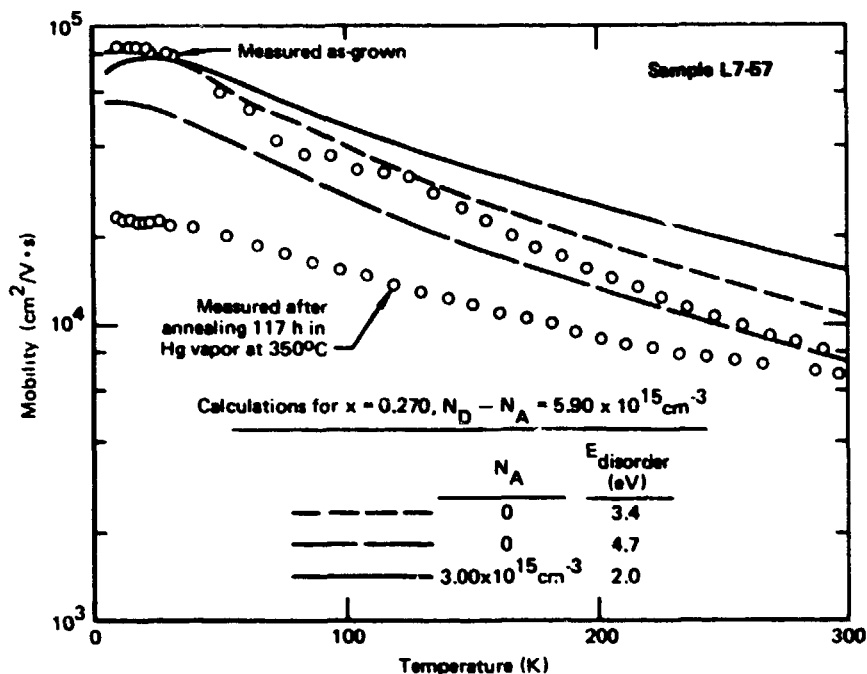
GP11-0818-8

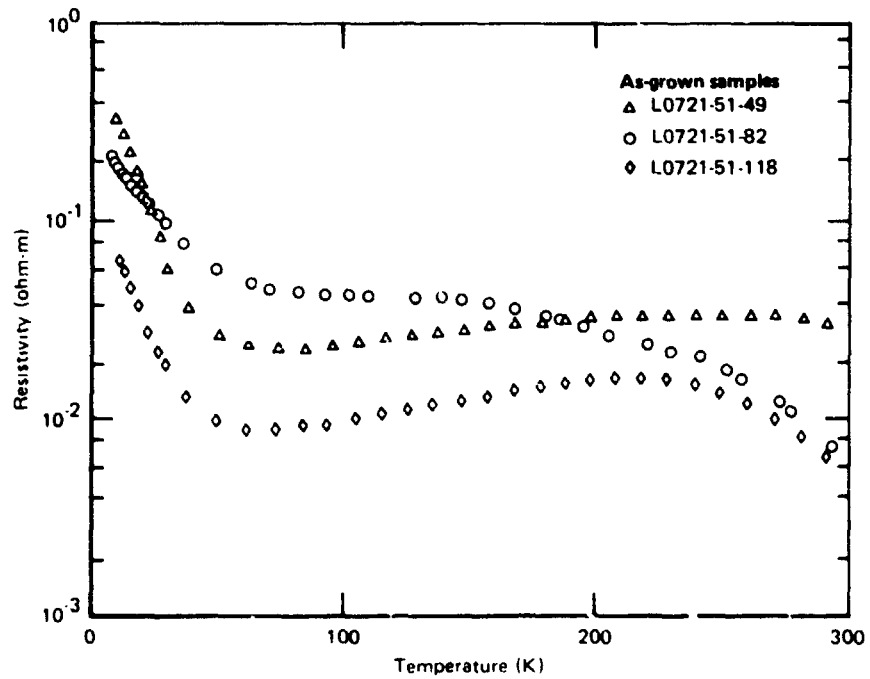Figure 20. Electron mobility as a function of temperature for sample L7-57.

The mobility at low temperatures in sample L7-57 following annealing
shows a large reduction, which implies a large increase in the defect concen-
trations in the sample as the result of annealing. A more complete evaluation
of this result will require further experimentation and theoretical analysis.

The measured Hall coefficients and resistivities for as-grown samples
from ingot L0721-51 are shown in Figures 21 and 22. In agreement with previ-
ously published results[20] for $Hg_{0.62}Cd_{0.38}Te$ samples with $N_A - N_D$ slightly
larger than 10^{16} cm^{-3}, the Hall coefficients below about 50 K show acceptor
freezeout with activation energies of 9-10 meV.
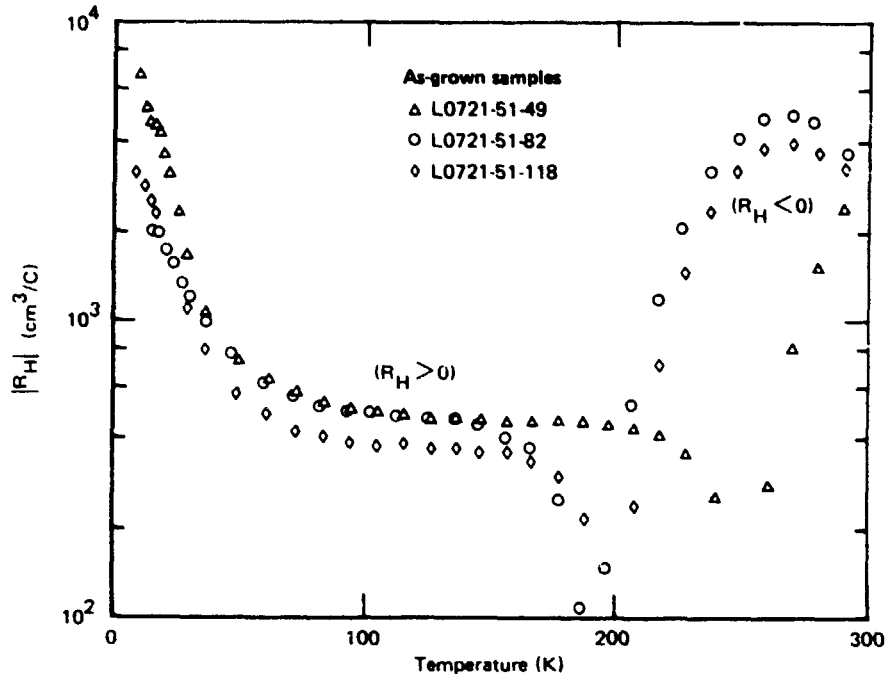
Figure 21. Temperature dependence of Hall coefficient for as-grown samples
L0721-51-49, L0721-51-82, and L0721-51-118.

Figure 22. Temperature dependence of resistivity for as-grown samples
L0721-51-49, L0721-51-82, and L0721-51-118.

28

Figures 23-26 show the temperature dependence of the Hall coefficients and resistivities of samples L0721-51-49 and L0721-51-118 following various annealings in an Hg atmosphere. The annealing parameters are given in Table 6. The choice of the parameters was based on data given in References 21 and 22. The temperature dependences of the Hall coefficients and resistivities indicate that the carrier concentrations in the samples did not reach equilibrium values during any of the annealings. Specifically, the temperature dependence of the Hall coefficients in Figures 23 and 25 cannot be explained on the basis of a homogeneous sample. Apparently, much longer annealing times are required to achieve carrier equilibration than the times employed.
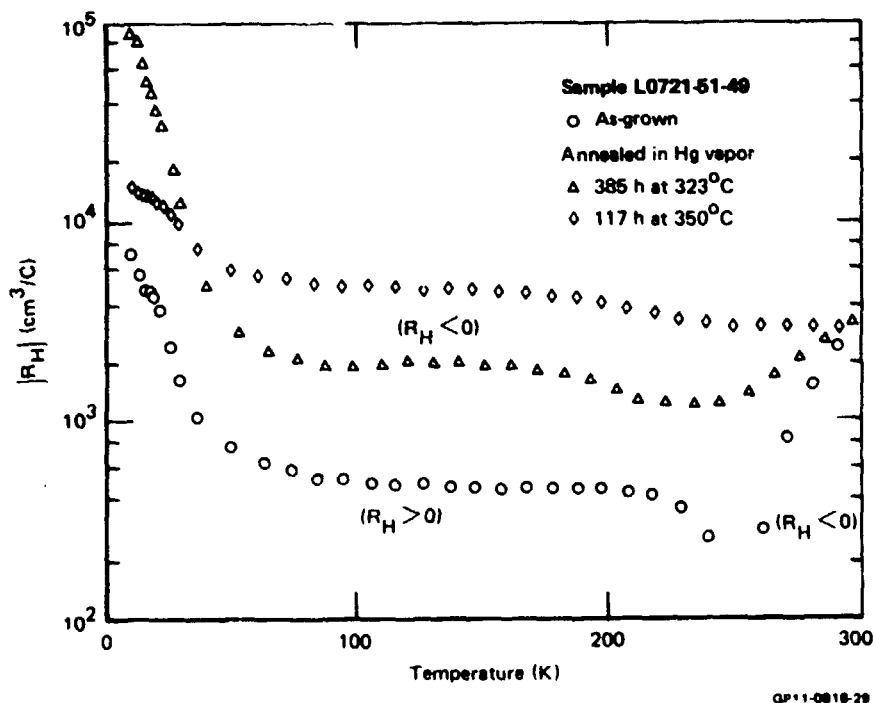

OP-11-0818-29

Figure 23. Temperature dependence of Hall coefficient for sample L0721-51-49.
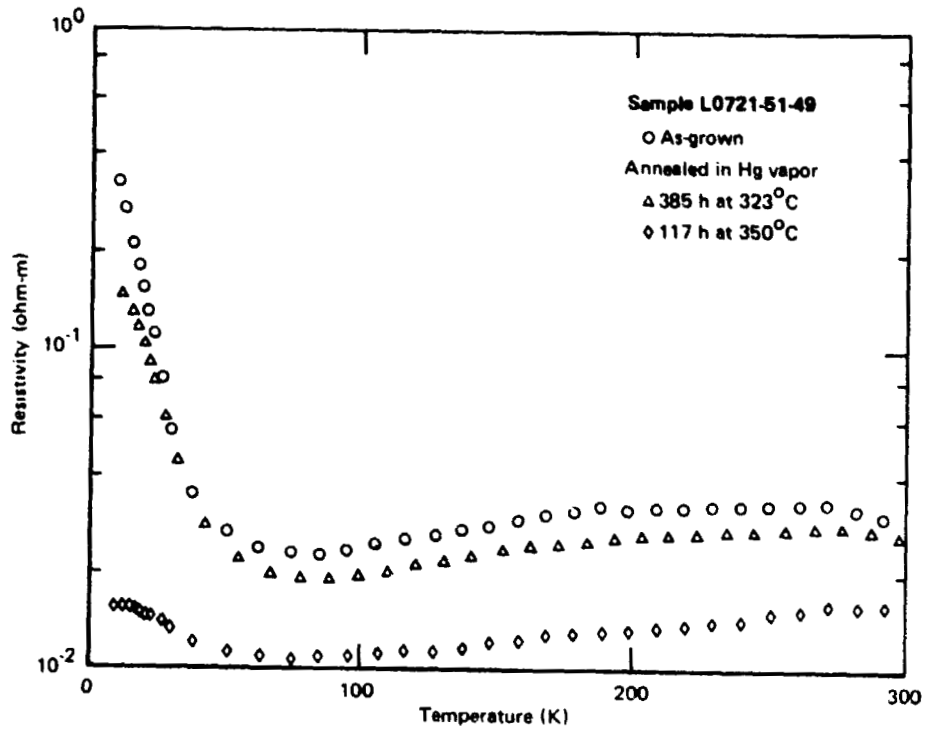
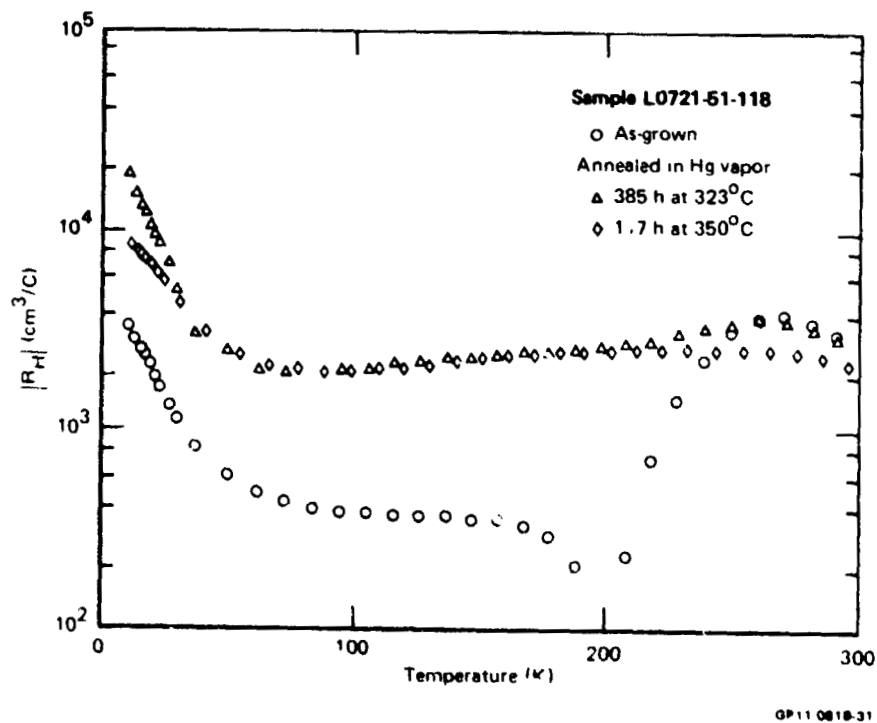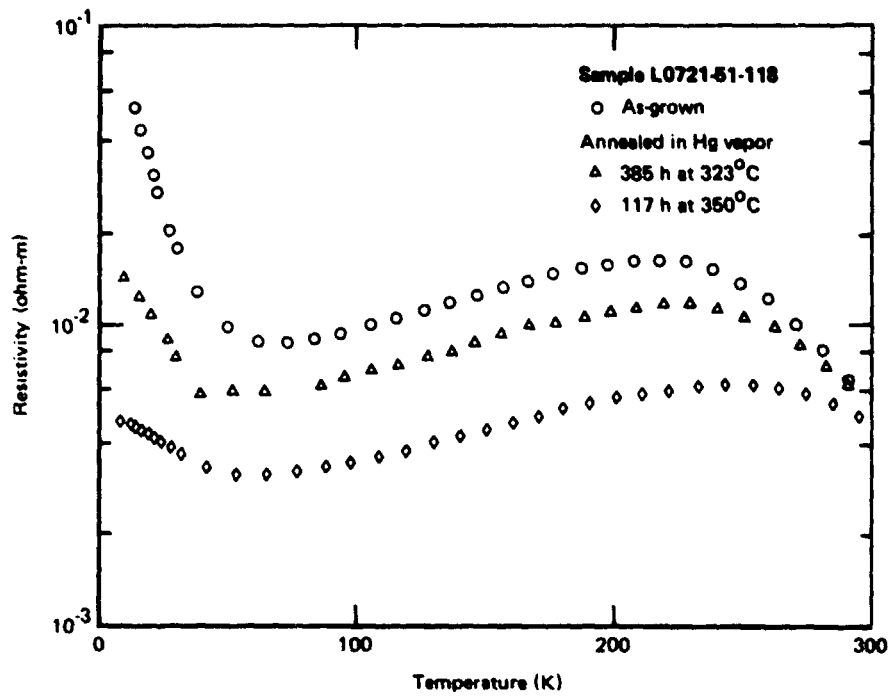**Figure 24. Temperature dependence of resistivity for sample L0721-51-49.**

Figure 25. Temperature dependence of Hall coefficient for sample L0721-51-118.

30

Figure 26. Temperature dependence of resistivity for sample L0721-51-118.

REFERENCES

1. S. L. Lehoczky, F. R. Szofran, and B. G. Martin, Advanced Methods for Preparation and Characterization of Infrared Detector Materials, McDonnell Douglas Corporation Report MDC Q0717 (5 July 1980), (Final Report for the period 5 December 1978 - 5 July 1980 for the George C. Marshall Space Flight Center Contract No. NAS8-33107).

2. F. R. Szofran and S. L. Lehoczky, The HgTe-CdTe Pseudobinary Phase Diagram, 22nd Annual Electronic Materials Conference, Ithaca, New York, 24-27 June 1980; Journal of Electronic Materials (in press).

3. S. L. Lehoczky, C. J. Summers, and F. R. Szofran, Directional Solidification and Characterization of $Hg_{1-x}Cd_xTe$ (x < 0.25), NATO Cadmium Mercury Telluride (CMT) Workshop, Grenoble, France, 23-24 April 1980.

4. A. S. Jordan, A Theory of Regular Associated Solutions Applied to the Liquidus Curves of the Zn-Te and Cd-Te Systems, Met. Trans. $\underline{1}$, 239 (1970).

5. S. Szapiro, Solid-Liquid Equilibria in Ternary Regular Associated Solutions, J. Electron. Mat. $\underline{5}$, 223 (1976).

6. A. J. Strauss, M.I.T. Lincoln Lab., private communication.

7. B. M. Kulwicki, The Phase Equilibria of Some Compound Semiconductors by DTA Calorometry, Ph.D. Dissertation, Univ. of Michigan (1963).

8. M. R. Lorenz, Phase Equilibria in the System Cd-Te, J. Phys. Chem. Solids $\underline{23}$, 939 (1962).

9. Jacques Steininger, Alan J. Strauss, and Robert F. Brebrick, Phase Diagram of the Zn-Cd-Te Ternary Systems, J. Electrochem. Soc. $\underline{117}$, 1305 (1970).

10. Jacques Steininger, Hg-Cd-Te Phase Diagram Determination by High Pressure Reflux, J. Electronic Mat. $\underline{5}$, 299 (1976).

11. V. G. Smith, W. A. Tiller, and J. W. Rutter, A Mathematical Analysis of Solute Redistribution During Solidification, Can. J. Phys. $\underline{33}$, 723 (1953).

12. S. L. Lehoczky and F. R. Szofran, Diffusion-Limited Directional Solidification of $Hg_{0.8}Cd_{0.2}Te$, Fifth International Conference on Vapor Growth and Fifth American Conference on Crystal Growth, Coronado, California, 19-24 July 1981.

13. S. L. Lehoczky, J. G. Broerman, D. A. Nelson, and C. R. Whitsett, Temperature-Dependent Electrical Properties of HgSe, Phys. Rev. B 9, 1598 (1974).

14. D. A. Nelson, J. G. Broerman, C. J. Summers, and C. R. Whitsett, Electrical Transport in the $Hg_{1-x}Cd_xSe$ Alloy System, Phys. Rev. B 18, 1658 (1978).

15. E. O. Kane, Band Structure of Indium Antimonide, J. Phys. Chem. Solids 1, 249 (1957).

16. Tse Tung, L. Golonka, and R. F. Brebrick, Thermodynamic Analysis of the HgTe-CdTe-Te System Using the Simplified RAS Model, J. Electrochem. Soc. 128, 1601 (1981).

17. F. Rosenberger, Fundamentals of Crystal Growth I (Springer-Verlag, Berlin, Heidelberg, New York, 1979), p. 305.

18. C. E. Chang and W. R. Wilcox, Control of Interface Shape in the Vertical Bridgman-Stockbarger Technique, J. Crystal Growth 21, 135 (1974).

19. L. J. van der Pauw, A Method of Measuring Specific Resistivity and Hall Effects of Discs of Arbitrary Shape, Philips Research Reports 13, 1 (1958).

20. W. Scott, E. L. Stelzer, and R. J. Hager, Electrical and Far-Infrared Optical Properties of p-Type $Hg_{1-x}Cd_xTe$, J. Appl. Phys. 47, 1408 (1976).

21. J. L. Schmit and E. L. Stelzer, The Effect of Annealing Temperature on the Carrier Concentrations of $Hg_{0.6}Cd_{0.4}Te$, J. Electronic Mat. 7, 65 (1978).

22. H. H. Shimizu, Improving the Properties of Cadmium Mercury Telluride, Ger. Offen. 2, 720, 891 in Chemical Abstracts 88; 82728x, 581 (1978).